*Article*

# Sedimentary Environment and Enrichment of Organic Matter in the Shahejie Formation, Huanghekou Depression, Bohai Bay Basin, China

**Zhenjie Jia [1,2], Dujie Hou [1,2,*] and Jiahao He [1,2]**

[1]  School of Energy Resources, China University of Geosciences, Beijing 100083, China; jiazhenjie0114@sina.com (Z.J.); 3006230011@email.cugb.edu.cn (J.H.)

[2]  Key Laboratory of Marine Reservoir Evolution and Hydrocarbon Accumulation Mechanism, Ministry of Education, China University of Geosciences, Beijing 100083, China

*  Correspondence: houdj313@163.com

**Abstract:** As a hydrocarbon-rich depression within the Bohai Bay Basin, the Huanghekou Depression is a focal region for exploring hydrocarbons in the eastern China Sea. Previous studies have insufficiently examined the correlation between the enrichment of organic matter and the environments in which it is deposited. Herein, the hydrocarbon potential, palaeoclimate, sedimentary environment, organic matter sources, and organic matter enrichment of the source rocks of the Shahejie Formation in the Huanghekou Depression were investigated using organic and inorganic geochemical indicators. The organic matter type of the source rock in Huanghekou Depression's Shahejie Formation was predominantly Type II, with a minor presence of Type III. Furthermore, the source rock had a poor-to-good comprehensive evaluation grade in $E_3s_{1-2}$, whereas $E_2s_3$ and $E_2s_4$ had medium-to-good comprehensive evaluations in their source rocks. In terms of maturity, $E_3s_1$ was in an intermediate position between the immature and mature stages and $E_3s_2$ and $E_2s_3$ were between the low-maturity and mature stages, whereas $E_2s_4$ transitioned into full maturity. Biomarkers and sensitive element indicators indicated that the organic matter in $E_3s_{1-2}$ was primarily derived from lower aquatic organisms and algae. This palaeoclimate was characterised by aridity, a water body containing saline and semi-saline water, and a strongly reducing environment resulting from water body stratification, leading to oxygen deficiency. The organic matter in $E_2s_3$ was primarily derived from aquatic organisms and algal inputs; these deposits were formed in a reduced environment characterised by relatively low salinity, ranging between semi-saline and freshwater conditions. The organic matter enrichment model of the Shahejie Formation was established based on sedimentary environment, palaeoclimatic, and organic matter source analyses, utilising $E_3s_{1-2}$ as preservation models and $E_2s_3$ as the productivity model. This study provides a basis for in-depth exploration and advancement of oil and gas reserves.

**Keywords:** sedimentary environment; Shahejie Formation; organic matter enrichment; Huanghekou Depression

## 1. Introduction

As global energy consumption surges and traditional onshore oil and gas reserves deplete, China's unconventional and offshore energy resources are receiving increasing attention. The Bohai Bay Basin is one of the richest oil-producing basins in eastern China [1] and boasts abundant petroleum resources, with confirmed oil reserves of approximately 13 billion tons and natural gas reserves of 351 billion cubic meters [2–4]. In the Huanghekou Depression, a hydrocarbon-abundant depression within the Bohai Bay Basin, significant oil fields, such as Bozhong29, Bozhong35-2, Bozhong34-9, and Kenli6-1, have been successfully discovered since the commencement of oil and gas exploration in 1980. As of 2020, 16 oil and gas fields have been discovered in the Huanghekou Depression, encompassing over 140 oil

and gas reservoirs with a combined third-level reserve volume reaching 890 million tons and dissolved gas reserves amounting to approximately 47.39 billion tons [5]. The predominant lithology of the Huanghekou Depression in the Cenozoic was sandy mudstone, which underwent sedimentation within a lake basin setting. Additionally, the variation in water depth exhibits multiple cycles, and geological conditions exist that are conducive to the development of multiple sets of source rocks [6]. The primary focus of development lies in four sets of source rocks, progressing from the lowermost to the uppermost layers, namely, the Kongdian Formation (Ek), the first through third members of the Shahejie Formation ($E_3s_{1-2}$, $E_2s_3$), and the third member of the Dongying Formation ($E_3d_3$). The thickness centre is primarily located in the northwest subdepression, the southwest subdepression, and the east depression [6]. Dark mudstone predominantly occurred in the middle parts of the $E_2s_3$, $E_3s_1$, and $E_3d_3$ formations. The Huanghekou Depression has been extensively studied by previous researchers in terms of the characteristics of its hydrocarbon source rocks, the potential for hydrocarbon accumulation, the formation characteristics of reservoirs, and reservoir development [7–12]. Zhuang et al. (2010) analysed the formation environment of mud shale; the palaeoenvironment was a hot and humid climate, and palaeoproductivity was high in $E_2s_3$. It was formed in a semi-deep-to-deep lake characterised by partially saline water bodies [6]. Liu and Wu et al (2007, 2015) comprehensively evaluated hydrocarbon source rocks in the Huanghekou Depression and concluded that the $E_2s_3$ and $E_3s_1$ formations exhibit favourable characteristics, such as good organic matter (OM) types and high thermal maturity, making them highly promising prospects for hydrocarbon generation [13,14]. Sun et al. (2011) examined the hydrocarbon accumulation levels and degree of accumulation in the study area, focusing on its structural, fault-related, and sequence-related aspects. The findings suggest that the oil and gas exhibit late-charging characteristics [15].

The formation of source rocks with excellent hydrocarbon quality is widely acknowledged to be controlled by the sedimentary environment. In recent years, abundant research has been conducted on sedimentary environment factors that influence OM formation. Changes in the sedimentary environment have direct implications for water body depth, lake basin development, plant community evolution, and detrital material transport [16,17]. Currently, various researchers are employing diverse methodologies for sedimentary environment reconstruction, including biomarker analysis, inorganic geochemical techniques, palaeontological fossil examinations, and palynological studies. Commonly utilised parameters for sedimentary environment assessment include palaeoclimatic conditions, bathymetric depth variations, salinity fluctuations, redox environment changes, and provenance determination [18–22]. The Huanghekou Depression has abundant oil and gas resources, and the Shahejie Formation is a key layer for oil and gas exploration. Previous studies on sedimentary environments have primarily relied on single indices, such as biomarkers, trace elements, and isotopes; moreover, extensive studies on the correlation between the enrichment of organic matter and the environments in which it is deposited are insufficient [6,13]. In light of prior research and considering the tectonic context of the region, this study aimed to analyse the sedimentary environment of the source rocks in the Huanghekou Depression within the Shahejie Formation using organic and inorganic geochemical methods. This study elucidates the mechanism underlying OM enrichment in this formation and establishes a model for its formation and enrichment.

## 2. Geological Setting

The Huanghekou Depression is situated beyond the estuary of the Yellow River (Figure 1a) in eastern China and encompasses a total area of approximately 3300 km$^2$ [23–26]. It shares borders with the Miaoxi Depression to the east and the Chengbei Depression and Zhanhua Depression to the west [25]. Its boundaries are defined by the Bonan Low Uplift to the north and the Laibei Low Uplift to the south (Figure 1b,c). This depression takes on a double-fault-like structure that was formed through mutual control exerted by both branches of the Tanlu Fault and an east–west strike-controlled fault [23–26]. The

Huanghekou Depression underwent a Palaeogene syn-rift subsidence phase, followed by a Neogene post-rift thermal subsidence stage during its Cenozoic evolution [27]. Fractures in southern Bohai Bay developed extensively during the Palaeogene syn-rift subsidence period, with common occurrences of strike–slip, normal, and strike–slip–extensional super-position faults. The Huanghekou Depression is primarily characterised by the development of two sets of fractures with near-EW and NNE strikes, which partition the basin into several secondary tectonic units: the northwest subdepression, southwest subdepression, the Central Tectonic Transformation Zone, and the east subdepression [15]. Within the four secondary tectonic units of the Huanghekou Depression, the northwest subdepression has a greater intensity than the eastern subdepression [15,28,29].
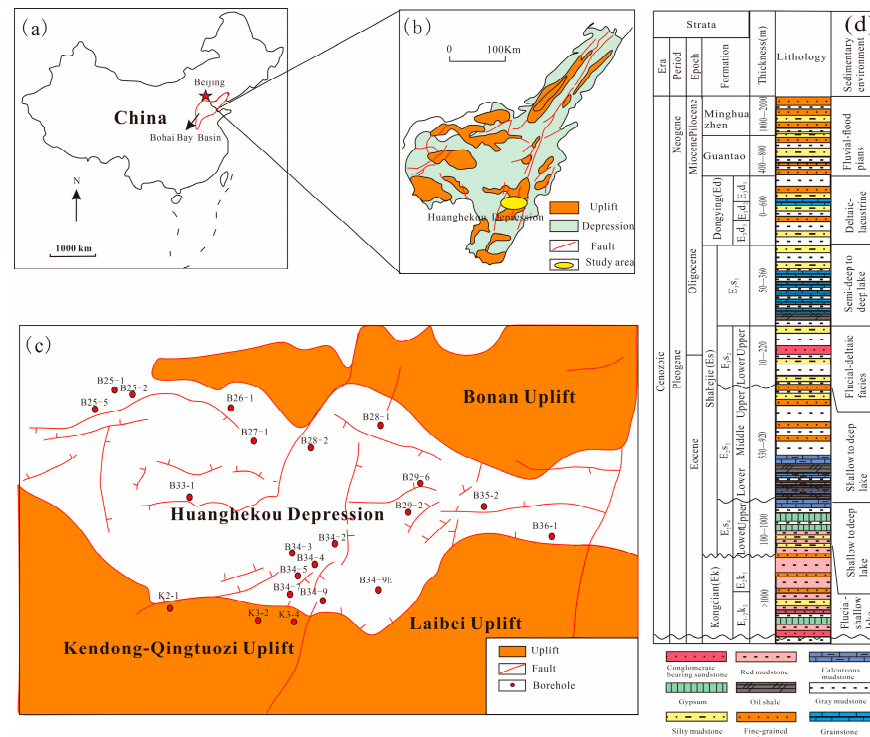


**Figure 1.** Map showing the regional geological outline of Bohai Bay Basin, Huanghekou Depression. (**a**) Location of study area in China; (**b**) regional tectonic units of Bohai Bay Basin, Huanghekou Depression; (**c**) structural units of study area and location of wells sampled here; and (**d**) generalised lithology, stratigraphy, and depositional environment of Bohai Bay Basin.

The thickness of Cenozoic sediments in the Huanghekou Depression reaches a substantial 4000 m. The strata comprise the Kongdian (Ek), Shahejie (Es), Dongying (Ed), Guantao (Ng), and Minghuazhen (Nm) Formations. Lithology mainly includes conglomerate-bearing sandstone, gypsum, silty mudstone, red mudstone, oil shale, fine-grained sandstone, calcareous mudstone, grey mudstone, and grainstone (Figure 1d). The mud shale in the Huanghekou Depression is substantially thick, indicating an extensive expansion of the lake basin, while the first member of the Shahejie Formation ($E_3s_1$) was deposited. This has resulted in the development of a shallow, widely distributed lake, wherein the cap layer exhibits maximum distribution, which is primarily characterised by a combination of thick mudstone and sandy mudstone with a thickness of less than 100 m; it has a strong capping ability. The second member of the Shahejie Formation ($E_3s_2$) is characterised by the predominance of fan deltaic–shallow lake deposits and exhibits interbedding made of sandy mudstone. The third member of the Shahejie Formation ($E_2s_3$) underwent the significant development of deep lacustrine facies and fan delta deposits, characterised by thick black and dark grey shales with a wide stratigraphic distribution and substantial

thickness. The predominant lithology is mudstone, which serves as the primary cap rock for deep oil reservoirs [3,5,30].

## 3. Samples and Methods

All materials and samples were obtained from the Tianjin Branch of the China National Offshore Oil Corporation (Tianjin, China). In total, 155 source rock samples from 22 wells were included in this study: 34 samples from the $E_3s_1$ formation (13 wells), 32 samples from the $E_3s_2$ formation (12 wells), 83 samples from the $E_2s_3$ formation (17 wells), and 6 samples from the $E_2s_4$ formation (2 wells). The spatial distribution of each well is shown in Figure 1. A comprehensive overview of the data ranges and sample quantities for total organic carbon (TOC), vitrinite reflectance (Ro), and pyrolysis measurements conducted on the rock samples from the Bohai Bay Basin is presented in Table 1.

**Table 1.** Geochemical parameters of rock samples in the Huanghekou Depression.

| Well | Depth (m) | Shahejie Formation | TOC (%) Average | Ro (%) Average | $T_{max}$ (°C) Average | $I_H$ (mg HC/g·TOC) Average | $S_1 + S_2$ (mg/g) Average |
|---|---|---|---|---|---|---|---|
| B25-1 | 3593–3600 | $E_2s_4$ | 2.84 | 0.57 | 443.33 | 302.15 | 10.01 |
| B25-2 | 3359.2–3660.2 | $E_2s_3$ | 3.3 | 1.07 | 436.25 | 417.43 | 16.53 |
| B25-5 | 3543.81–3684.5 | $E_2s_3$ | 4.76 | 0.72 | 439.33 | 614.79 | 41.79 |
| B26-1 | 3550–3640 | $E_2s_3$ | 3.07 | 0.6 | 441.75 | 513.31 | 19.22 |
| B27-1 | 3710–3730 | $E_3s_1$ | 0.76 | 0.9 | 448 | 205.44 | 1.86 |
| | 3790–3860 | $E_3s_2$ | 0.92 | 0.98 | 447 | 211 | 2.33 |
| | 3890 | $E_2s_3$ | 1.02 | 1.15 | 449 | 200 | 2.37 |
| | 3920–3950 | $E_2s_4$ | 1.19 | 1.18 | 449.33 | 161.45 | 2.43 |
| B28-2 | 3325–3375 | $E_3s_2$ | 0.98 | 0.57 | 411 | 587.57 | 6.37 |
| | 3400–3600 | $E_2s_3$ | 2.96 | 0.61 | 433.33 | 471.99 | 15.45 |
| B28-1 | 3190–3250 | $E_3s_1$ | 2.6 | 0.64 | 441.25 | 594.81 | 18.28 |
| | 3270–3290 | $E_3s_2$ | 2.17 | 0.65 | 440.5 | 569.9 | 15.07 |
| | 3320–3640 | $E_2s_3$ | 2.6 | 0.63 | 442.09 | 402.99 | 13.75 |
| B29-6 | 3000–3070 | $E_3s_1$ | 1.47 | 0.47 | 441 | 379.07 | 6.39 |
| | 3120–3170 | $E_3s_2$ | 2.24 | 0.53 | 443.5 | 396.5 | 10.12 |
| | 3220–3450 | $E_2s_3$ | 2.46 | 0.57 | 442.6 | 332.52 | 10.16 |
| B29-2 | 2690–2720 | $E_3s_1$ | 2.11 | 0.46 | 436 | 574.95 | 12.75 |
| | 2750 | $E_3s_2$ | 0.89 | 0.49 | 442 | 423.6 | 4.11 |
| | 2780–2840 | $E_2s_3$ | 1.34 | 0.56 | 439.33 | 388.24 | 6.56 |
| B33-1 | 3600 | $E_3s_1$ | 0.9 | 0.6 | 435 | 306.67 | 3.03 |
| | 3800–3975 | $E_2s_3$ | 3.09 | 0.62 | 438.38 | 352.47 | 13.81 |
| B34-2 | 3365.5 | $E_2s_3$ | 0.96 | 0.48 | 440 | 225 | 2.28 |
| B34-3 | 3550–3650 | $E_2s_3$ | 0.5 | 0.58 | 443.67 | 148.34 | 0.99 |
| | 3450–3500 | $E_3s_2$ | 0.53 | 0.49 | 442.5 | 203.06 | 1.36 |
| B34-4 | 3276.7 | $E_3s_1$ | 0.68 | 0.4 | 441 | 199.71 | 1.56 |
| B34-5 | 3276–3297.5 | $E_3s_1$ | 0.61 | 0.32 | 445.5 | 208.43 | 1.47 |
| B34-7 | 3035 | $E_3s_1$ | 11.6 | 0.31 | 436 | 808.19 | 95.68 |
| B34-9 | 2980–3020 | $E_3s_1$ | 1.07 | 0.64 | 440 | 426.37 | 5.04 |
| | 3060–3140 | $E_3s_2$ | 0.76 | 0.64 | 443.5 | 471.59 | 4.3 |
| | 3220–3500 | $E_2s_3$ | 1 | 0.66 | 447.57 | 415.99 | 4.15 |
| B34-9E | 3010–3180 | $E_3s_2$ | 0.35 | 0.6 | 413.5 | 574.4 | 1.63 |
| B35-2 | 2700–2750 | $E_3s_1$ | 0.87 | 0.5 | 435.33 | 200.26 | 1.92 |
| | 2770–2820 | $E_2s_3$ | 0.61 | 0.56 | 434.33 | 261.76 | 2 |
| | 2900–2950 | $E_2s_3$ | 1.45 | 0.51 | 438 | 390.51 | 7 |

**Table 1.** *Cont.*

| Well | Depth (m) | Shahejie Formation | TOC (%) Average | Ro (%) Average | $T_{max}$ (°C) Average | $I_H$ (mg HC/g·TOC) Average | $S_1 + S_2$ (mg/g) Average |
|------|-----------|--------------------|-----------------|----------------|------------------------|-----------------------------|----------------------------|
| B36-1 | 2260 | $E_2s_3$ | 2.5 | 0.46 | 434 | 513.2 | 13.25 |
| K2-1 | 3300–3380 | $E_3s_1$ | 0.7 | 0.71 | 445 | 242.37 | 2.04 |
| | 3420–3500 | $E_3s_2$ | 0.8 | 0.64 | 444.67 | 226.83 | 2.94 |
| | 3540–3700 | $E_2s_3$ | 1.13 | 0.67 | 446 | 268.22 | 3.51 |
| K3-2 | 2800–2890 | $E_3s_1$ | 0.66 | 0.6 | 422.71 | 273.94 | 1.93 |
| | 2900–2970 | $E_3s_2$ | 0.67 | 0.65 | 372 | 297.42 | 2.12 |
| | 3000–3210 | $E_2s_3$ | 0.9 | 0.71 | 393.36 | 314.89 | 3.03 |
| K3-4 | 3110–3200 | $E_3s_1$ | 0.42 | 0.58 | 433.25 | 269.97 | 1.35 |
| | 3290–3390 | $E_2s_3$ | 0.75 | 0.64 | 433.6 | 295.16 | 2.63 |
| | 3420 | $E_2s_3$ | 1.16 | 0.74 | 411 | 258.63 | 3.72 |

Note: "Depth" represents the buried depth of each sample with a deduction of water depth; TOC: total organic carbon; $S_1 + S_2$: free hydrocarbons + potential hydrocarbons; Ro: vitrinite reflectance; $T_{max}$: temperature of maximum hydrocarbon generation rate.

The source rock samples were pretreated with deionised water and ethanol to eliminate surface contaminants. Subsequently, the samples were pulverised to a particle size of 100 mesh, weighed for various experiments, and analysed for TOC using a American Leco CS344 Analyser designed specifically for determining carbon and sulphur contents. Subsequently, approximately 100-mesh powder samples were subjected to rock pyrolysis for a semi-process test, resulting in the acquisition of unbound hydrocarbons ($S_1$), prospective hydrocarbons ($S_2$), and maximum generation ($T_{max}$). A German Leica MV-SP microphotometer equipped with an oil-immersed objective lens was used to measure Ro. The values were calibrated using the dual-Ro standard dual-calibration method. If the measurement deviation of the standard sample exceeded ±0.02%, the sample was re-measured. The aliphatic hydrocarbon fractions in the hydrocarbon source rocks were analysed with gas chromatography–mass spectrometry (GC-MS) using an American Agilent 7890A gas chromatograph equipped with a DB5ms fused silica capillary column (length: 60 m, inner diameter: 0.25 mm, film thickness: 0.25 μm). Additionally, an American Agilent 5975C mass-selective detector with an ionisation energy of 70 eV was employed. The vaporisation temperature of the inlet was adjusted to 300 °C, and the sample was introduced without any division at a consistent flow rate of 1.5 mL/min, utilising helium as the carrier gas. The initial temperature of the oven was set at 50 °C and maintained for 1 min. Subsequently, it underwent a programmed increment of 20 °C/min until it reached a maximum temperature of 120 °C. There was subsequently a gradual elevation over 30 min to attain a final temperature of 300 °C. The samples were subjected to testing in full-scan mode. The main elements were determined using X-ray fluorescence spectrometry and achieved an analytical accuracy of over 98%, while inductively coupled plasma mass spectrometry was used to determine trace and rare earth elements, ensuring an analytical precision exceeding 95%.

## 4. Results

### 4.1. Rock-Eval Pyrolysis, Vitrinite Reflectance Data, and Source Rock Quality

In $E_3s_1$ of the Huanghekou Depression, the TOC average value was 1.88%. In $E_3s_2$ of the study area, the TOC average value was 1.03%. Further, in $E_2s_3$ of the study area, the TOC average value was 1.87%, while in $E_2s_4$, the TOC average value was 2.01% (Table 1).

A comprehensive assessment of the source rocks in the study area showed that the predominant organic matter types could be classified as Type $II_2$ in $E_3s_{1–2}$, indicating poor source rock and good source rock, while in $E_2s_3$, the dominant organic matter types could be categorised as Type $II_1$–$II_2$, with a minor presence of Type III, suggesting poor source rock and good source rock, and in $E_2s_4$, the primary organic matter types consisted mainly of Type $II_2$ accompanied by a small amount of Type III, indicating medium source rock and

good source rock (Figure 2a,b). The Ro analysis of the source rock indicated that $E_3s_1$ of the Huanghekou Depression was between the immature and mature stages, $E_3s_2$ was in the low-maturity-to-mature stage, and $E_2s_3$ was also between the low-maturity and mature stages, whereas $E_2s_4$ reached the mature stage (Figure 2c).
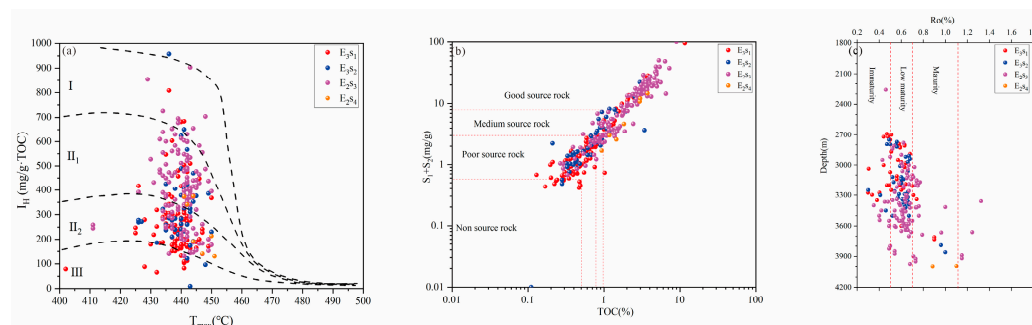


**Figure 2.** Comprehensive evaluation of source rock. (**a**) Plot of $I_H$ versus $T_{max}$ evaluating organic matter types; (**b**) TOC content versus rock-eval $S_1 + S_2$, showing the hydrocarbon generation potential of the samples; and (**c**) plot of vitrinite reflectance versus depth evaluating the maturity of samples from the Shahejie Formation in the Huanghekou Depression.

*4.2. Biomarker Compounds*

The distribution pattern of *n*-alkanes in the source rocks of the Shahejie Formation in the Huanghekou Depression was predominantly characterised as the front-peak type, with few samples exhibiting the bimodal type. In the mass chromatogram, at *m/z* 85, the distribution of detected *n*-alkanes in the Huanghekou Depression samples predominantly ranged from $C_{12}$ to $C_{33}$, exhibiting distinct variations across different strata. The carbon number distribution of *n*-alkanes in $E_3s_{1-2}$ exhibited a relatively comprehensive profile, characterised by a prominent front peak and occasional bimodal features. The main peak ranged from $C_{16}$ to $C_{25}$, while the odd–even dominance index (OEP) ranged from 0.77 to 1.81 (average: 1.16), and the average chain length (ACL) ranged from 12.67 to 23.50 (average: 17.09) (Table 2). The carbon number distribution of the *n*-alkanes predominantly fell within the $C_{12}$–$C_{30}$ range in $E_2s_3$, exhibiting a front-peak distribution pattern, while some samples displayed a bimodal characteristic, with the main peak ranging from $C_{15}$ to $C_{23}$, OEP values ranging from 0.84 to 2.08 (average: 1.16), and an ACL ranging from 12.82 to 20.54 (average: 17.78) (Table 2). The analysed samples contained a significant abundance of isoprenoids, including pristane (Pr) and phytane (Ph) (Figure 3 and Table 2).

**Table 2.** Related parameters of normal alkanes and isoprenoids in the studied area.

| Well | OEP Average | ACL Average | Ph/nC$_{18}$ Average | Pr/nC$_{17}$ Average | Pr/Ph Average |
|---|---|---|---|---|---|
| B25-1 | 1.07 | 17.88 | 0.41 | 0.59 | 1.5 |
| B25-2 | n.d. | n.d. | n.d. | n.d. | n.d. |
| B25-3 | 1.12 | 17.29 | 0.32 | 0.43 | 1.21 |
| B25-5 | n.d. | n.d. | n.d. | n.d. | n.d. |
| B26-1 | 1.35 | 17.39 | 1.68 | 1.4 | 1.24 |
| B27-1 | 1.12 | 18.47 | 0.19 | 0.43 | 2.1 |
| B28-1 | 1.19 | 18.5 | 0.35 | 0.81 | 1.4 |
| B28-2 | 1.14 | 17.65 | 0.28 | 0.49 | 1.77 |
| B29-6 | n.d. | n.d. | n.d. | n.d. | n.d. |
| B29-2 | 1.2 | 16.49 | 0.62 | 0.93 | 1.75 |
| B29-3 | 1.34 | 19.34 | 0.49 | 0.82 | 3.44 |
| B33-1 | 1.1 | 18.24 | 0.46 | 0.47 | 1.45 |
| B34-1 | 1.16 | 17.8 | 0.33 | 0.52 | 0.78 |
| B34-2 | 1.14 | 18.23 | 0.31 | 0.43 | 1.33 |
| B34-3 | 1.14 | 17.76 | 0.28 | 0.43 | 1.35 |
| B34-5 | 1.18 | 15.36 | 0.41 | 1.01 | 1.38 |

**Table 2.** *Cont.*

| Well | OEP Average | ACL Average | Ph/nC$_{18}$ Average | Pr/nC$_{17}$ Average | Pr/Ph Average |
|------|-------------|-------------|----------------------|----------------------|---------------|
| B34-6 | 1.12 | 15.26 | 0.69 | 1.52 | 1.41 |
| B34-7 | 1.15 | 16.31 | 0.38 | 0.66 | 1.28 |
| B34-9 | 1.16 | 16.96 | 0.47 | 0.81 | 1.06 |
| B34-9A | 1.12 | 15.75 | 0.56 | 1.06 | 1.94 |
| B34-9E | 1.13 | 16.34 | 1.21 | 1.28 | 1.58 |
| B36-1 | 1.51 | 14.47 | 1.97 | 1.42 | 0.75 |
| K2-1 | 1.16 | 18.2 | 0.42 | 0.75 | 1.66 |
| K3-2 | 1.17 | 14.37 | 0.75 | 0.65 | 2.28 |
| K4-1 | 1.12 | 18.99 | 0.9 | 1.1 | 1.62 |

Note: OEP: odd-to-even predominance = $\left[\left(C_{max-2} + 6 \times C_{max} + C_{max+2}/(4C_{max-1} + 4C_{max+1})\right)\right]^{(-1)^{max-1}}$ alkanes; ACL: average chain length = $\sum(n \times Cn)/\sum Cn$; n is among 15–33; Pr: pristane; Ph: phytane; n.d.: no data.
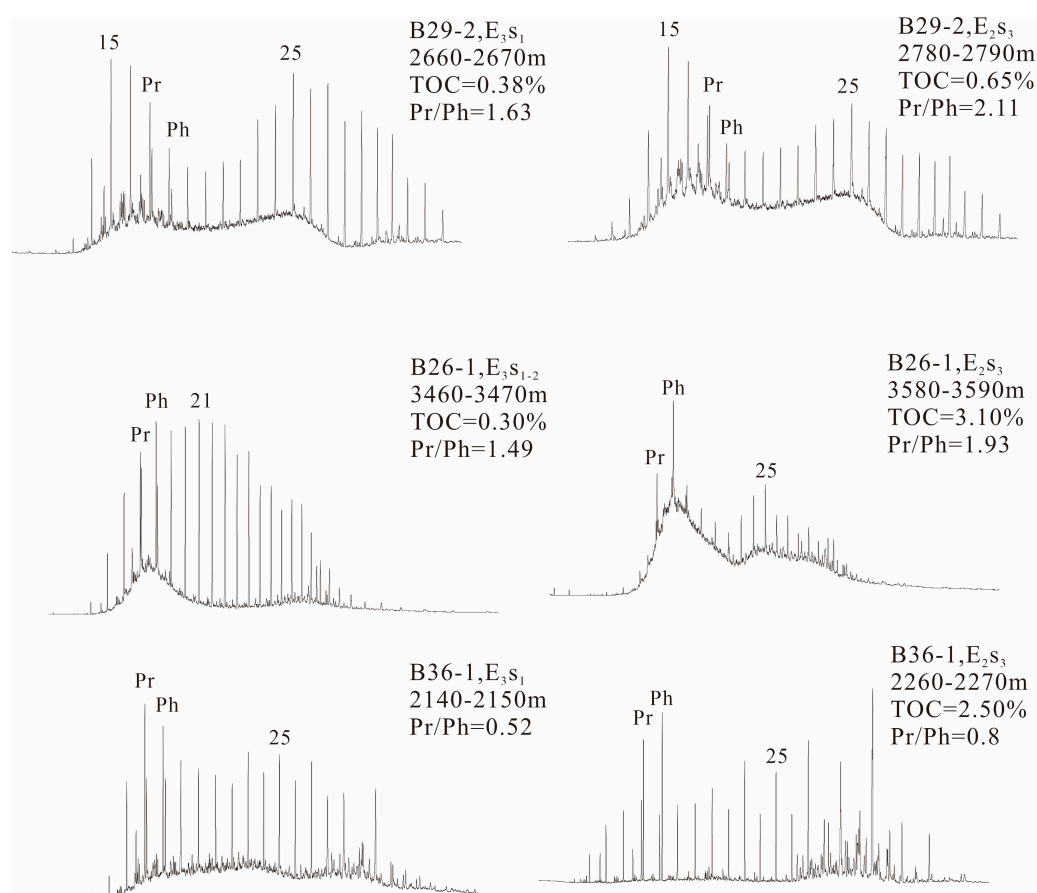


**Figure 3.** Partial *m/z* 85 mass chromatograms showing the distributions of n-alkanes in the source rock from the Huanghekou Depression.

The steranes identified in the Shahejie Formation of the Huanghekou Depression were predominantly regular steranes, rearranged steranes, and 4-methylsteranes. However, the reason for the rearrangement of steranes remains largely unknown. Based on the monitoring of mass chromatograms (*m/z* 217), all samples exhibited similar characteristics in the distribution of steranes, primarily featuring the configuration of (20R) -5α(H), 14α(H), and 17α(H). Among these, C$_{27}$ steranes had the highest relative content (0.09–0.74%), followed by C$_{29}$ (0.04–0.72%) and C$_{28}$ steranes (0.06–0.37%), indicating a trend of C$_{27}$ > C$_{29}$ > C$_{28}$ (Figure 4 and Table 3).
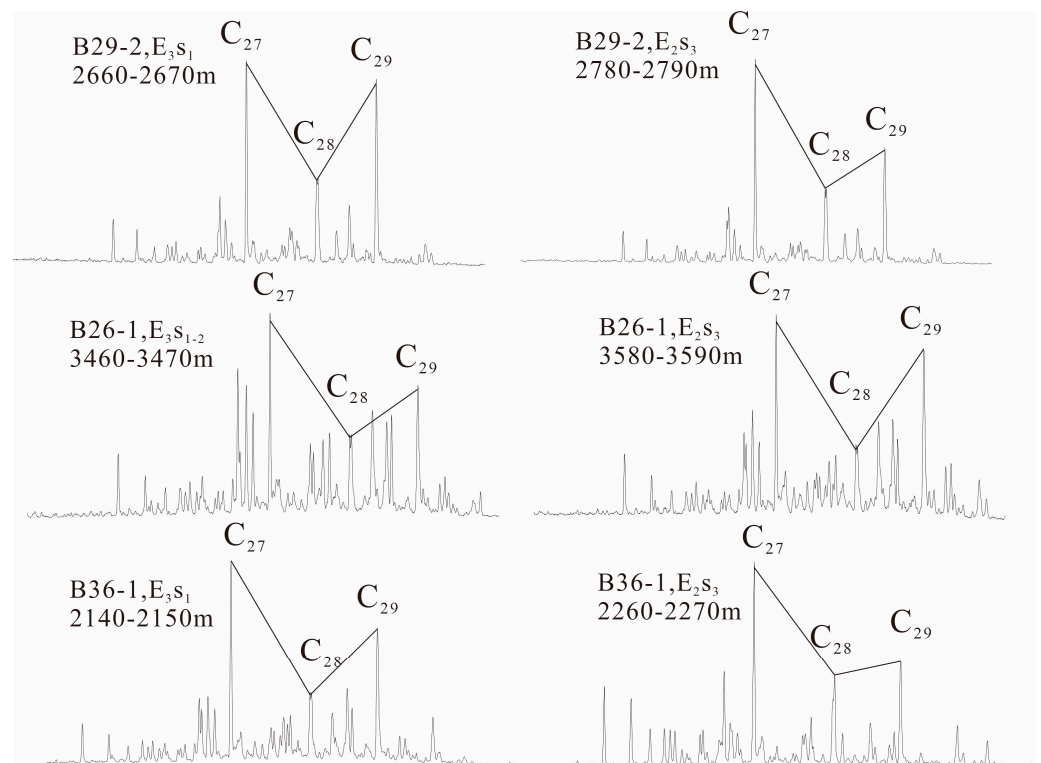
**Figure 4.** Partial *m/z* 217 mass chromatograms showing the sterane distributions in the rock extracts from the Huanghekou Depression.

**Table 3.** Terpene- and sterane-related parameters in the studied area.

| Well | Ga/C$_{30}$Hop Average | C$_{27}$ Steranes Average | C$_{28}$ Steranes Average | C$_{29}$ Steranes Average |
|---|---|---|---|---|
| B25-1 | n.d. | n.d. | n.d. | n.d. |
| B25-2 | 0.1 | 0.23 | 0.18 | 0.59 |
| B25-3 | n.d. | n.d. | n.d. | n.d. |
| B25-5 | 0.05 | 0.29 | 0.24 | 0.48 |
| B26-1 | 0.11 | 0.37 | 0.12 | 0.5 |
| B27-1 | 0.24 | 0.44 | 0.24 | 0.32 |
| B28-1 | n.d. | n.d. | n.d. | n.d. |
| B28-2 | n.d. | n.d. | n.d. | n.d. |
| B29-6 | 0.54 | 0.35 | 0.17 | 0.48 |
| B29-2 | 0.12 | 0.48 | 0.16 | 0.36 |
| B29-3 | 0.14 | 0.48 | 0.25 | 0.27 |
| B33-1 | n.d. | n.d. | n.d. | n.d. |
| B34-1 | 0.42 | 0.18 | 0.22 | 0.59 |
| B34-2 | n.d. | n.d. | n.d. | n.d. |
| B34-3 | n.d. | n.d. | n.d. | n.d. |
| B34-5 | 0.22 | 0.23 | 0.2 | 0.58 |
| B34-6 | n.d. | n.d. | n.d. | n.d. |
| B34-7 | 0.4 | 0.59 | 0.16 | 0.25 |
| B34-9 | 0.05 | 0.31 | 0.09 | 0.6 |
| B34-9A | 0.17 | 0.45 | 0.14 | 0.42 |
| B34-9E | n.d. | n.d. | n.d. | n.d. |
| B36-1 | 0.1 | 0.45 | 0.17 | 0.38 |
| K2-1 | 0.12 | 0.52 | 0.17 | 0.31 |
| K3-2 | 0.53 | 0.45 | 0.24 | 0.32 |
| K4-1 | 0.45 | 0.46 | 0.09 | 0.45 |

Note: Ga/C$_{30}$Hop: gammacerane/C$_{30}$ $\alpha\beta$ hopane; C$_{27}$ steranes = C$_{27}$ steranes/(C$_{27}$ steranes + C$_{28}$ steranes + C$_{29}$ steranes); C$_{28}$ steranes = C$_{28}$ steranes/(C$_{27}$ steranes + C$_{28}$ steranes + C$_{29}$ steranes); C$_{29}$ steranes = C$_{29}$ steranes/(C$_{27}$ steranes + C$_{28}$ steranes + C$_{29}$ steranes); n.d.: no data.

### 4.3. Major and Trace Elements

In recent years, increasing advancements in inorganic geochemical testing techniques have increased the popularity of utilising primary trace elements, rare earth elements, and isotopes to reveal sedimentary palaeoenvironments in oil and gas geology. Consequently, numerous significant achievements have been made in this field. The elemental compositions of the source rocks of the Huanghekou Depression in the Shahejie Formation are listed in Table 4.

**Table 4.** The concentration of major and trace elements in the studied area.

| Shahejie Formation | $SiO_2$ (%) Average | $Al_2O_3 + K_2O + Na_2O$ (%) Average | Co (μg/g) Average | V/(V + Ni) (μg/g) Average | V/Cr (μg/g) Average |
|---|---|---|---|---|---|
| $E_3s_1$ | 50.02 | 19.42 | 15.68 | 0.74 | 0.69 |
| $E_2s_3$ | 50.37 | 16.92 | 23.5 | 0.71 | 1.12 |
|  | MgO/CaO (%) | C Value | $K_2O/Al_2O_3$ (%) | V/Ni (μg/g) |  |
| $E_3s_1$ | 1.92 | n.d. | n.d. | 3.01 | n.d. |
| $E_2s_3$ | 0.42 | 0.51 | 0.24 | 2.41 | n.d. |

Note: n.d.: no data.

## 5. Discussion

### 5.1. Organic Matter Sources

Biomarkers have been extensively utilised to identify organic matter sources. Saturated hydrocarbons and *n*-alkanes serve as the most commonly used indices [31–37]. *n*-alkanes, being the simplest compounds found in sedimentary organic matter, play a crucial role in investigating hydrocarbon source rocks and are widely employed as indicators to determine the depositional palaeoenvironments and parent material types associated with source rock formations [35]. For instance, *n*-alkanes exhibit front-peak distribution characteristics with a low main peak carbon number, suggesting that the organic matter originates primarily from aquatic organisms and algae. Conversely, *n*-alkanes displaying post-peak distribution characteristics with a high main peak carbon number indicate that the organic matter is predominantly derived from terrigenous higher plants [31–38]. If *n*-alkanes exhibit a bimodal distribution, organic matter is suggested to be derived from a blend of various resources, encompassing both lesser aquatic organisms and higher plants from terrestrial environments. Additionally, the carbon preference index (CPI), average chain length (ACL), and terrigenous/aquatic ratio (TAR) have been extensively employed to discern the sources of organic matter [34,38–40]. Generally, $C_{27}$–$C_{29}$ regular steranes are the most prevalent and widely used compounds, and their relative content serves as an indicator of the input information from the organic source [41]. The presence of $C_{27}$ steranes implies that the origins of the parent material are lower aquatic organisms and algae, whereas $C_{29}$ steranes indicate a higher plant source [41–44].

The organic matter in $E_3s_{1–2}$ and $E_2s_3$ in the study area exhibited characteristics of mixed-source input, indicating the existence of both lower aquatic organisms and terrigenous higher plants. However, the contributions from these two sources differed significantly. The *m/z* 85 mass chromatograms (Figure 3) demonstrated that $E_3s_{1–2}$ exhibited a front-peak distribution, with some displaying bimodal features. Similar traits were observed in $E_2s_3$, suggesting that the organic matter present in both $E_3s_{1–2}$ and $E_2s_3$ originated primarily from lower aquatic organisms. A cross-map of Ph/n$C_{18}$ and Pr/n$C_{17}$ [28] revealed that the organic matter in the Shahejie Formation originated from a mixture of sources, with some contributions derived from terrigenous higher plants. The *m/z* 217 mass chromatograms (Figure 4) demonstrated a distinctive distribution pattern of $C_{27}$-$C_{28}$-$C_{29}$ regular steranes, forming an asymmetric "V" shape with the order of abundance as $C_{27} > C_{29} > C_{28}$. The dominance of $C_{27}$ regular steranes suggested a significant contribution from lower aquatic organisms in the $E_3s_{1–2}$ and $E_2s_3$ samples. A ternary diagram (Figure 5) revealed that all available samples were a concentrated cluster, indicating a mixture of terrestrial and

aquatic organic matter sources, as evidenced by the relative proportions of $C_{27}$, $C_{28}$, and $C_{29}$ steranes.
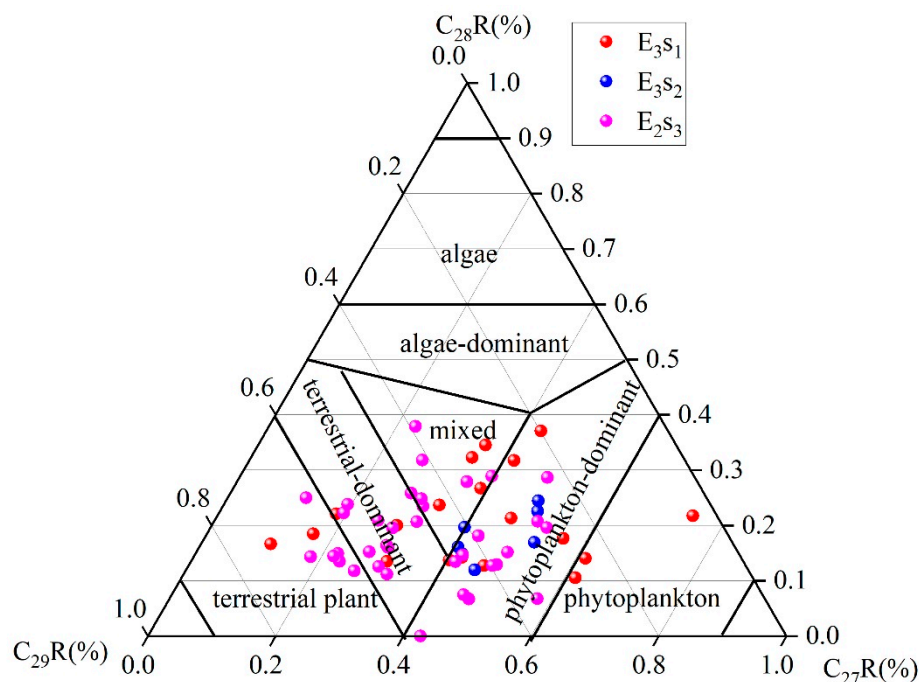


**Figure 5.** Ternary diagram of the $C_{27}$-$C_{28}$-$C_{29}$ $\alpha\alpha\alpha$ 20R steranes for the source rock in the study area, showing the source of the OM.

*5.2. Deposition Environment*

Commonly used biomarker parameters include isoprene alkanes such as pristane and phytane; chlorophylls produced through photosynthesis in green plants; and purple sulphur compounds found in bacterial chlorophylls that can also generate pristane and phytane [41]. Phytols formed in chlorophyll and phytoliths can be transformed into pristanes and phytanes under specific redox conditions, thereby demonstrating their potential for evolution. This ratio is frequently employed to indicate the parent material of the hydrocarbon source rock and depositional environment. Abundant pristane and phytane were detected in the samples collected from the Huanghekou Depression of the Shahejie Formation. The former was utilised to classify the sedimentary environment of source rocks using $Ph/nC_{18}$-$Pr/nC_{17}$ [41] and the geochemical parameters of the source rocks within the Shahejie Formation in Huanghekou Depression, and the $Ph/nC_{18}$ versus $Pr/nC_{17}$ cross-plot suggested that the Shahejie Formation was deposited in varied and blended settings, featuring partially Type II and Type III organic matter in reducing and oxidising environments, respectively, as well as a mixture of different types of OM in transitional environments (Figure 6). The geochemistry of elements is also responsive to changes in the palaeoenvironment, and alterations in the redox conditions of sedimentary water resulted in the fractionation of variable-valence elements, thereby causing element redistribution. Significant advancements have been made in the use of elemental geochemistry for sedimentary environment analyses. The commonly used indicators for identifying oxygen-poor and anoxic environments include $V/(V + Ni)$, $V/Cr$, $U/Th$, $Ni/Co$, and $V/Sc$ [45]; for example, an environment is considered anaerobic when $V/(V + Ni)$ is less than 0.6, while a reducing environment is indicated by a $w(V)/w(V + Ni)$ ranging between 0.6 and 0.84, and a $(V)/w(V + Ni)$ value greater than 0.84 indicates a strongly reducing environment. Further, $V/Cr$ values less than 2 indicate an oxygen-abundant environment, whereas $V/Cr$ values between 2 and 4.25 suggest oxygen scarcity. Conversely, $V/Cr$ values exceeding 4.25 indicate an anoxic environment [45–48]. According to the cross-diagram of Co and $V/(V + Ni)$, as well as those illustrating $V/(V + Ni)$ and $V/Cr$ (Figure 7a,b),

the depositional environment of $E_3s_1$ was characterised by an oxygen-poor and anoxic sulphide environment, and that of $E_2s_3$ was a sub-oxygen-poor environment. Generally, $E_3s_1$ displayed higher reducibility through the geochemical indices of elements.
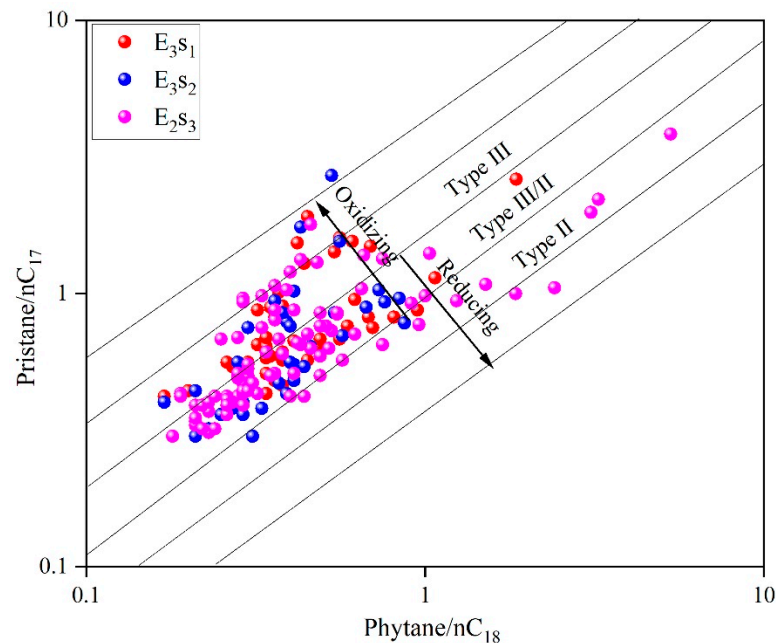


**Figure 6.** Relationship between $Ph/nC_{18}$ and $Pr/nC_{17}$ ratio values for samples from the Shahejie Formation in the Huanghekou Depression of the Bohai Bay Basin, showing the source of the OM.
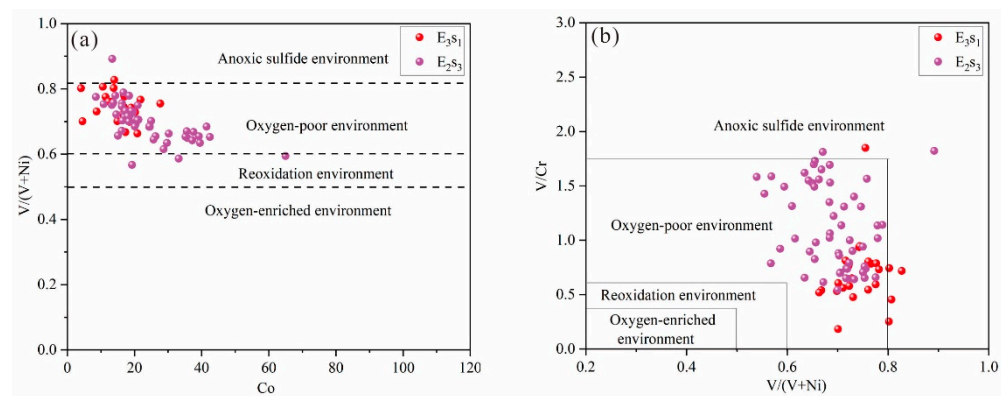


**Figure 7.** Cross-plot of element geochemistry for samples from the Shahejie Formation in the Huanghekou Depression of the Bohai Bay Basin. (**a**) The Co and $V/(V + Ni)$ cross-plot; (**b**) The $V/(V + Ni)$ and $V/Cr$ cross-plot, showing the palaeoenvironment of the samples.

Ga is a $C_{30}$-banded naphthene derived from tetrahymenolol and serves as a significant molecular marker for water stratification [49]. The stratification of water became more pronounced with increasing $Ga/C_{30}Hop$ levels. This can be observed through the Gammacerane index ($Ga/C_{30}Hop$) (Table 3). The $Ga/C_{30}Hop$ values in $E_3s_1$, $E_2s_3$, and $E_2s_3$ ranged from 0.05 to 0.73 (average: 0.24), 0.50 to 1.62 (average: 0.23), and 0.02 to 0.19 (average: 0.15), respectively. The higher $Ga/C_{30}Hop$ of $E_3s_1$ suggested that organic matter was deposited in water during a period characterised by salinity stratification, as indicated by the mean values provided above. A cross-map (Figure 8) utilising the $Pr/ph$ and Ga indices revealed that the salinity of the water body during the deposition period of $E_3s_{1-2}$ was relatively elevated, ranging from saline to brackish conditions. Conversely, the salinity of the water body during the deposition period of $E_2s_3$ was comparatively low, ranging from freshwater to brackish conditions. The V/Ni ratio can also serve as an indicator of water column

salinity. In general, if the V/Ni ratio exceeds 1, it indicates a brackish water environment, with higher ratios corresponding to higher salinity [50]. The V/Ni ratio in $E_3s_1$ and $E_2s_3$ ranged from 1.97 to 4.79 (average: 3.01) and 1.17 to 8.25 (average: 2.41), respectively, as shown in Table 4. Additionally, the geochemical indicators of these elements suggested that the salinity of the water in $E_3s_1$ was higher than that in $E_2s_3$.
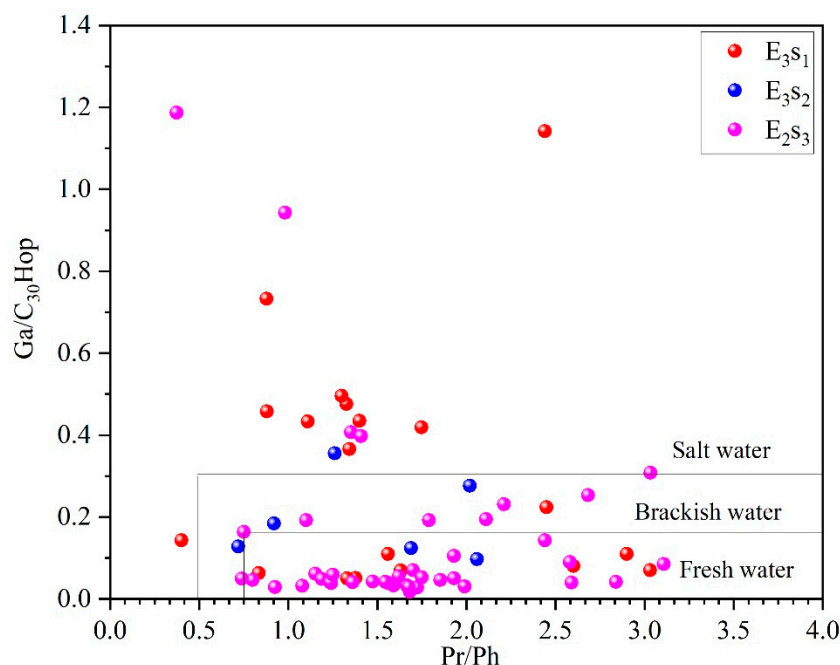


**Figure 8.** Cross-plot of Pr/ph and gammacerane index for samples from the Shahejie Formation, in the Huanghekou Depression of the Bohai Bay Basin, showing water salinity in the palaeoenvironment of the samples.

### 5.3. Palaeoclimate

Climate change significantly influences the formation of source rocks because of its impact on precipitation patterns, lake dynamics, water stratification, and salinity variation to some extent [41–45]. The composition of metallic elements in sediments varies under different climatic conditions. Therefore, parameters, such as the Cu content of metal elements, Sr/Cu ratio, Fe/Cu ratio, and palaeoclimate index C values are commonly employed to reflect the palaeoclimate [51]. The elemental geochemistry method has been utilised to discuss changes in palaeoclimate [51–53]. The MgO/CaO value of limestone serves as a reliable indicator of climate change, with a higher MgO/CaO ratio suggesting hot and arid climatic conditions and a lower ratio indicating wetter climate conditions [52]. The MgO/CaO ratio in $E_3s_1$ and $E_2s_3$ of the Huanghekou Depression ranged from 0.21 to 5.35 (average: 1.92) and 0.12 to 1.29 (average: 0.42), respectively (Table 4). These findings suggest a relatively arid climate during the sedimentary period of $E_3s_1$. The depositional period of $E_2s_3$ was characterised by a relatively warm and humid climate. The migration and enrichment patterns of elements varied under different climatic conditions. In arid climates, Ca, Mg, Na, Ba, Sr, and K are favoured for enrichment, whereas, in humid climates, Fe, Ni, Co, Cr, Mn, and V are favoured [46]. Therefore, these two elemental indicators of arid and humid climates can be employed to reflect the palaeoclimate, with the ratio of the two being recorded as the palaeoclimate index "C-value". This index was calculated using the following formula: C = w(V + Ni + Mn + Fe + Cr + Co)/w(Ca + Mg + Ba + Sr + Na + K). A C-value greater than 0.6 indicates a warm and humid climate, while a C-value less than 0.2 indicates a dry and hot climate [54]. The available data indicated that the C-value in $E_2s_3$ ranged from 0.36 to 0.73 (average: 0.51), presenting additional support for a climate characterised by high humidity during the deposition period in $E_2s_3$. A discriminant map

of $Al_2O_3 + Na_2O + K_2O$ and $SiO_2$ (Figure 9) can also effectively elucidate the patterns of palaeoclimate evolution [55,56]. The $E_3s_1$ samples in the Huanghekou Depression were distributed in semi-humid and arid regions, while $E_2s_3$ samples were found in warm and humid climatic regions. However, climate evolution is a complex process, and relying solely on a single indicator may not be sufficient for an accurate assessment. The ACL method was employed to further validate the palaeoclimate of the Shahejie Formation. Generally, lower ACL values indicate higher precipitation and weaker evaporation, resulting in higher effective humidity and a relatively humid climate, whereas higher ACL values suggest lower precipitation and stronger evaporation, leading to lower effective humidity and a relatively arid climate. Considering Wells B29-2, B34-9, and B36-1 as examples (Figure 10), the ACL value was higher during the deposition period of $E_3s_1$, indicating a relatively arid climate; conversely, the ACL value was lower during the deposition period of $E_2s_3$, suggesting a warmer and more humid climate.



**Figure 9.** Cross-plot of $Al_2O_3 + Na_2O + K_2O$ and $SiO_2$ for samples from the Shahejie Formation, in the Huanghekou Depression of the Bohai Bay Basin, showing the palaeoclimate of the samples.
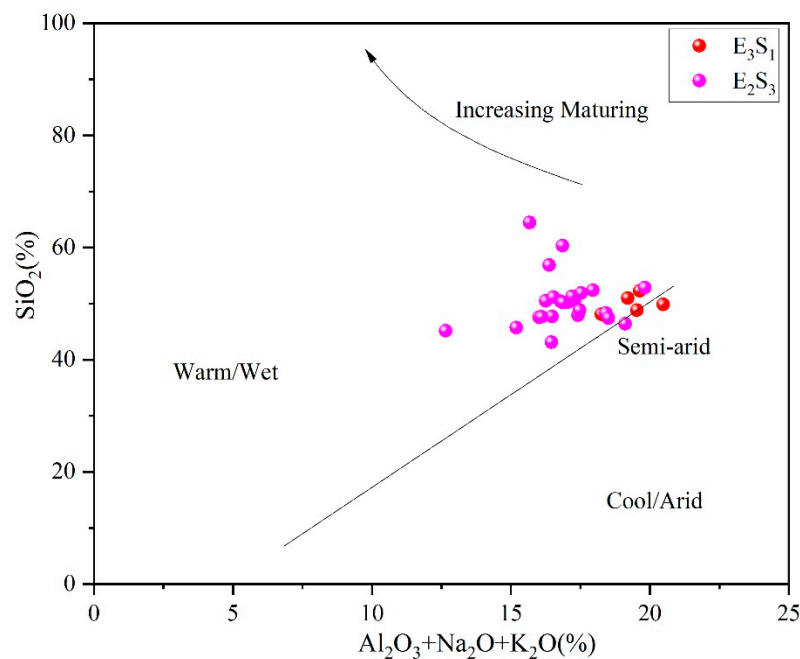


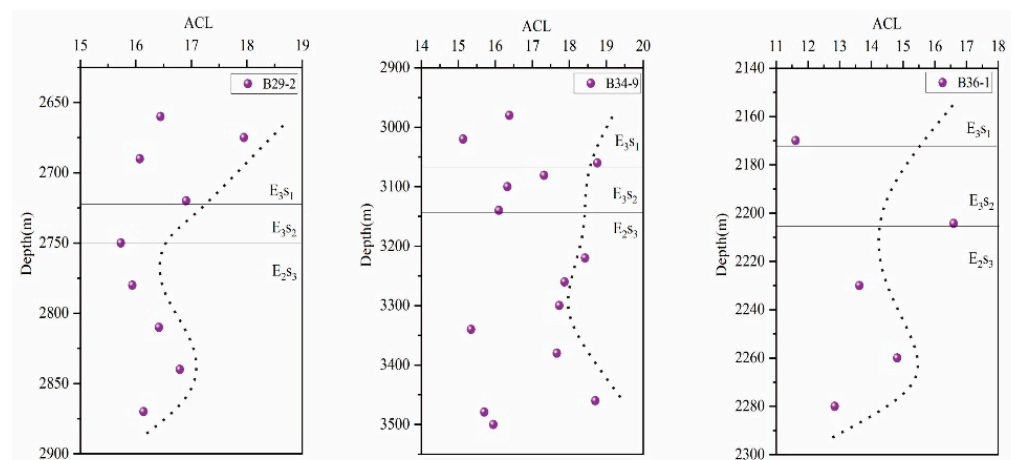**Figure 10.** Cross-plot of ACL and depth for samples from the Shahejie Formation in the Huanghekou Depression of the Bohai Bay Basin, showing the palaeoclimate of the samples.

### 5.4. Developmental Models for Source Rocks

The formation of lacustrine source rocks is influenced by factors such as the redox environment, productivity, preservation conditions, and the palaeoclimate. According to the aforementioned analysis of organic matter sources, sedimentary environments, and palaeoclimatic conditions, the source rock development model of the Shahejie Formation in the Huanghekou Depression can be categorised into two models: the preservation model of $E_3s_{1-2}$ and the productivity model of $E_2s_3$. During the depositional period of $E_3s_{1-2}$ (Figure 11), the lake basin experienced a stable phase characterised by gradual structural settlement and a low sedimentation rate [6]. The encroachment of the lake covered a large area, resulting in a shallow water body. Within the depression, there was widespread development of shallow shoreline lacustrine facies. In addition, terrigenous higher plants made only a relatively minor contribution to the organic matter content of the source rocks. Conversely, high water salinity promotes the occurrence of algal blooms. High salinity is also conducive to the formation of halocline from salinity difference and the development of a stable strong reduction environment, which is conducive to the preservation of organic matter. During the deposition of $E_2s_3$, the lake basin underwent active rifting characterised by a rapid sedimentation rate [6]. The encroachment area of the lake was extensive and characterised by a substantial water body and a warm and humid climate that facilitated the proliferation of aquatic organisms and algae, resulting in a high productivity level. The simultaneous introduction of a substantial volume of freshwater resulted in the influx of nutrients and higher plants, thereby decreasing the salinity of the aquatic environments. This subsequently created an anoxic reduction zone at the bottom of the lake basin, facilitating optimal conditions for organic matter preservation. At the same time, the semi-deep lake and deep lake are widely developed, and the water depth is large, which is conducive to the formation of an anoxic reduction environment at the bottom of the water body through temperature stratification.
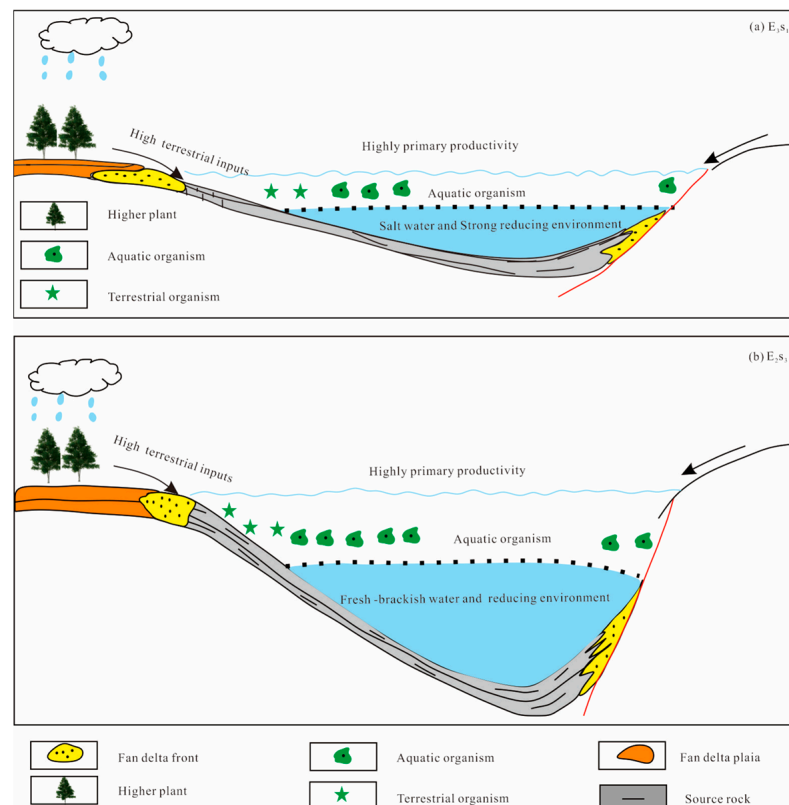


**Figure 11.** Organic matter enrichment model representing. (**a**) the preservation model of $E_3s_{1-2}$ and (**b**) the productivity model of $E_2s_3$.

## 6. Conclusions

Given the total organic carbon, rock-eval pyrolysis, vitrinite reflectance data, and source rock quality, these results show that the organic matter composition of source rocks in the Huanghekou Depression, specifically in $E_3s_{1-2}$, can be predominantly classified as Type $II_2$, while in $E_2s_3$, the predominant organic matter type is a combination of Types $II_1$ and $II_2$ with a minor presence of Type I. Lastly, in $E_2s_4$, the main organic matter type was identified as Type $II_2$ with a small amount of Type III. In terms of maturity, $E_3s_1$ was in an intermediate position between the immature and mature stages, while $E_3s_2$ and $E_2s_3$ were situated between the low-maturity and mature stages, and $E_2s_4$ transitioned into the stage of full maturity.

The sources of organic matter at different layers in the study area were analysed by using biomarker methods. In these methods, *n*-alkane- and sterane-related parameters are effectively used to distinguish terrigenous higher plants from aquatic organisms. The inorganic geochemical method is applied to the sedimentary environment, water salinity, and palaeoclimate of the study area. After conducting the aforementioned analysis, we postulated that the sedimentary organic matter of $E_3s_{1-2}$ in the Huanghekou Depression represents a mixed source, primarily of aquatic organisms, with a lesser contribution from terrigenous higher plants. It was deposited under strong reducing conditions, characterised by high water salinity and the presence of saline and semi-saline water bodies, which provided favourable preservation conditions for organic matter. The organic matter in $E_2s_3$ represented a mixed source, primarily of aquatic organisms. The source rocks were deposited under reducing conditions with relatively low salinity, ranging from semi-saline to freshwater. In $E_2s_3$, the climate during the sedimentary period was warm with abundant moisture, resulting in high palaeoproductivity.

The organic matter of the Shahejie Formation was influenced by different depositional environments and climates in distinct ways. These findings indicate that the organic material in the Shahejie Formation of the Huanghekou Depression was predominantly derived from aquatic organisms and algal sources, as evidenced by the discrimination indices for distinguishing between aquatic organisms and higher plants of terrestrial origin. However, the contributions of aquatic organisms and algae were higher in $E_2s_3$ than in $E_3s_{1-2}$. We further developed an organic matter enrichment model for the Huanghekou Depression. Specifically, $E_3s_{1-2}$ represented the preservation model, and $E_2s_3$ represented the productivity model.

**Author Contributions:** Z.J.: conceptualization, methodology, original draft preparation, reviewing, and editing; D.H.: visualization, investigation, supervision, validation, reviewing, and editing; J.H.: methodology, software, and validation. All authors have read and agreed to the published version of the manuscript.

**Institutional Review Board Statement:** Not applicable.

**Informed Consent Statement:** Not applicable.

**Data Availability Statement:** The datasets presented in this study can be obtained upon request to the corresponding author.

**Conflicts of Interest:** The authors declare no conflicts of interest.

## References

1. Chen, L.; Tian, J.; Cui, H.; Ma, X.; Song, X.; Yuan, Q.; Liu, J. Hydrocarbon generation mechanism of lamalginite- and telalginite-dominated source rocks in a saline lake basin: A case study of the Permian Lucaogou formation in the Jimusaer Sag, Junggar Basin. *Energy Geosci.* **2023**, *4*, 100191. [CrossRef]
2. Hao, F.; Zhou, X.; Zhu, Y.; Yang, Y. Lacustrine Source Rock Deposition in Response to Co-Evolution of Environments and Organisms Controlled by Tectonic Subsidence and Climate, Bohai Bay Basin, China. *Org. Geochem.* **2011**, *42*, 323–339. [CrossRef]
3. Hao, F.; Zhou, X.; Zhu, Y.; Zou, H.; Bao, X.; Kong, Q. Mechanisms of Petroleum Accumulation in the Bozhong Sub-Basin, Bohai Bay Basin, China. Part 1: Origin and Occurrence of Crude Oils. *Mar. Pet. Geol.* **2009**, *26*, 1528–1542. [CrossRef]
4. Hao, F.; Zou, H.; Gong, Z.; Deng, Y. Petroleum Migration and Accumulation in the Bozhong Sub-Basin, Bohai Bay Basin, China: Significance of Preferential Petroleum Migration Pathways (PPMP) for the Formation of Large Oilfields in Lacustrine Fault Basins. *Mar. Pet. Geol.* **2007**, *24*, 1–13. [CrossRef]
5. Sun, T.; Fu, G.; Lv, Y.F.; Hu, M.; Liu, Z.; Wang, H. Main controlling factors on the hydrocarbon accumulation in the middle-shallow layer of 1st structure, Nanpu Sag. *Nat. Gas Geosci.* **2014**, *25*, 1042–1051, (In Chinese with English Abstract)
6. Zhuang, X.; Zou, Y.; Jiang, X.; Yang, Y.; Sun, H. Development Mechanism of Lacustrine Source Rocks in Yellow River. *Sci. Technol. Rev.* **2010**, *28*, 48–54. (In Chinese with English Abstract)
7. Gong, L.; Wang, J.; Gao, S.; Fu, X.; Liu, B.; Miao, F.; Zhou, X.; Meng, Q. Characterization, Controlling Factors and Evolution of Fracture Effectiveness in Shale Oil Reservoirs. *J. Pet. Sci. Eng.* **2021**, *203*, 108655. [CrossRef]
8. Huang, H.; Pearson, M.J. Source Rock Palaeoenvironments and Controls on the Distribution of Dibenzothiophenes in Lacustrine Crude Oils, Bohai Bay Basin, Eastern China. *Org. Geochem.* **1999**, *30*, 1455–1470. [CrossRef]
9. Lan, X.; Liu, H. The Geochemical Characteristics of the Paleogene Lacustrine Source Rock and Cenozoic Oil in the Eastern Huanghekou Sag, Bohai Bay Basin, China: An Oil–Source Rock Correlation. *J. Pet. Sci. Eng.* **2022**, *214*, 110434. [CrossRef]
10. Wang, E.; Li, C.; Feng, Y.; Song, Y.; Guo, T.; Li, M.; Chen, Z. Novel Method for Determining the Oil Moveable Threshold and an Innovative Model for Evaluating the Oil Content in Shales. *Energy* **2022**, *239*, 121848. [CrossRef]
11. Peng, W.; Sun, H.; Zhang, R.; Yu, H.; Zhang, X. Later-stage near-source preponderent hydrocarbon pooling pattern in the Huanghekou Sag of the Bohai Sea waters. *Oil Gas Geol.* **2009**, *30*, 510–518. (In Chinese with English Abstract)
12. Chen, B.; Hao, F.; Zou, Y. Geochemical Character of the hydrocarbon in BZ26-2 Oilfield Bozhong Depression and its implication for petroleum accumulation. *J. Xi'an Shiyou Univ.* **2006**, 1–4+113. (In Chinese with English Abstract)
13. Liu, Z.; Li, S.; Xin, R.; Xu, C.; Cheng, J. Paleoclimatic information in stratigraphic records and its r elation to the formation of hydrocarbon source rocks—A case study of the Paleogene strata in the Huanghekou subbasin of the Bohai Bay basin, China. *Geollogical Bull. China* **2007**, *26*, 830–840. (In Chinese with English Abstract)
14. Wu, K.Q.; Jiang, X.; Sun, H. Model of lacustrine source rocks in offshore oil kitchen sags: A case study of paleogene in Huanghekou Sag. *Geol. Sci. Tecnol. Inf.* 2015; 34, 63–70. (In Chinese with English Abstract)
15. Sun, H.F.; Zhou, X.; Peng, W.X.; Zou, Y.; Yang, B.; Zeng, X. Late-stage hydrocarbon accumulation and enrichment in the Huanghekou Sag, southern Bohai Sea. *Pet. Explor. Dev.* **2011**, *38*, 307–313. (In Chinese with English Abstract)
16. Carroll, A.R.; Simon, C.; Graham, S.A. Brass Upper Permian Lacustrine Oil Shales, Southern Junggar Basin, Northwest China. *AAPG Bull.* **1992**, *76*, 1874–1902. [CrossRef]
17. Bradley, W.H. Oil Shale Formed in Desert Environment: Green River Formation, Wyoming. *Geol. Soc. Am. Bull.* **1973**, *84*, 1121. [CrossRef]
18. Jiang, Y.; Hou, D.; Li, H.; Zhang, Z.; Guo, R. Impact of the Paleoclimate, Paleoenvironment, and Algae Bloom: Organic Matter Accumulation in the Lacustrine Lucaogou Formation of Jimsar Sag, Junggar Basin, NW China. *Energies* **2020**, *13*, 1488. [CrossRef]
19. Liang, C.; Cao, Y.; Jiang, Z.; Wu, J.; Guoqi, S.; Wang, Y. Shale Oil Potential of Lacustrine Black Shale in the Eocene Dongying Depression: Implications for Geochemistry and Reservoir Characteristics. *AAPG Bull.* **2017**, *101*, 1835–1858. [CrossRef]
20. Wu, P.; Hou, D.; Gan, J.; Li, X.; Ding, W.; Liang, G.; Wu, B. Paleoenvironment and Controlling Factors of Oligocene Source Rock in the Eastern Deep-Water Area of the Qiongdongnan Basin: Evidences from Organic Geochemistry and Palynology. *Energy Fuels* **2018**, *32*, 7423–7437. [CrossRef]
21. Zeng, S.; Wang, J.; Fu, X.; Chen, W.; Feng, X.; Wang, D.; Song, C.; Wang, Z. Geochemical Characteristics, Redox Conditions, and Organic Matter Accumulation of Marine Oil Shale from the Changliang Mountain Area, Northern Tibet, China. *Mar. Pet. Geol.* **2015**, *64*, 203–221. [CrossRef]
22. Zhang, W.; Yang, W.; Xie, L. Controls on Organic Matter Accumulation in the Triassic Chang 7 Lacustrine Shale of the Ordos Basin, Central China. *Int. J. Coal Geol.* **2017**, *183*, 38–51. [CrossRef]
23. Li, S.Z.; Suo, Y.H.; Santosh, M.; Dai, L.M.; Liu, X.; Yu, S.; Zhao, S.J.; Jin, C. Mesozoic to Cenozoic Intracontinental Deformation and Dynamics of the North China Craton. *Geol. J.* **2013**, *48*, 543–560. [CrossRef]
24. Liu, H.; Xia, Q.; Somerville, I.D.; Wang, Y.; Zhou, X.; Niu, C.; Du, X.; Zhang, X. Paleogene of the Huanghekou Sag in the Bohai Bay Basin, NE China: Deposition-Erosion Response to a Slope Break System of Rift Lacustrine Basins: Slope Break System of Paleogene Rift Lacustrine Basins. *Geol. J.* **2015**, *50*, 71–92. [CrossRef]
25. Qi, J.; Yang, Q. Cenozoic Structural Deformation and Dynamic Processes of the Bohai Bay Basin Province, China. *Mar. Pet. Geol.* **2010**, *27*, 757–771. [CrossRef]
26. Tong, K.; Zhao, C.; Lü, Z.; Zhang, Y.; Zheng, H.; Xu, S.; Wang, J.; Pan, L. Reservoir Evaluation and Fracture Chracterization of the Metamorphic Buried Hill Reservoir in Bohai Bay Basin. *Pet. Explor. Dev.* **2012**, *39*, 62–69. [CrossRef]

27.  Hu, S.; O'Sullivan, P.B.; Raza, A.; Kohn, B.P. Thermal History and Tectonic Subsidence of the Bohai Basin, Northern China: A Cenozoic Rifted and Local Pull-Apart Basin. *Phys. Earth Planet. Inter.* **2001**, *126*, 221–235. [CrossRef]
28.  Cong, F.; Zhang, H.; Hao, F.; Xu, S. Direct Control of Normal Fault in Hydrocarbon Migration and Accumulation in Northwestern Bozhong Subbasin, Bohai Bay Basin, China. *Mar. Pet. Geol.* **2020**, *120*, 104555. [CrossRef]
29.  Liu, H.; Zhao, D.; Jiang, Y.; Zhuang, M.; Liu, Y. Hydrocarbon Accumulation Model for Neogene Traps in the Chengdao Area, Bohai Bay Basin, China. *Mar. Pet. Geol.* **2016**, *77*, 731–745. [CrossRef]
30.  Schultz, R.B. Geochemical Relationships of Late Paleozoic Carbon-Rich Shales of the Midcontinent, USA: A Compendium of Results Advocating Changeable Geochemical Conditions. *Chem. Geol.* **2004**, *206*, 347–372. [CrossRef]
31.  Ding, W.; Hou, D.; Gan, J.; Wu, P.; Zhang, M.; George, S.C. Palaeovegetation Variation in Response to the Late Oligocene-Early Miocene East Asian Summer Monsoon in the Ying-Qiong Basin, South China Sea. *Palaeogeogr. Palaeoclimatol. Palaeoecol.* **2021**, *567*, 110205. [CrossRef]
32.  Haberer, R.M.; Mangelsdorf, K.; Wilkes, H.; Horsfield, B. Occurrence and Palaeoenvironmental Significance of Aromatic Hydrocarbon Biomarkers in Oligocene Sediments from the Mallik 5L-38 Gas Hydrate Production Research Well (Canada). *Org. Geochem.* **2006**, *37*, 519–538. [CrossRef]
33.  Izart, A.; Suarez-Ruiz, I.; Bailey, J. Paleoclimate Reconstruction from Petrography and Biomarker Geochemistry from Permian Humic Coals in Sydney Coal Basin (Australia). *Int. J. Coal Geol.* **2015**, *138*, 145–157. [CrossRef]
34.  Jiang, L.; George, S.C. Biomarker Signatures of Upper Cretaceous Latrobe Group Hydrocarbon Source Rocks, Gippsland Basin, Australia: Distribution and Palaeoenvironment Significance of Aliphatic Hydrocarbons. *Int. J. Coal Geol.* **2018**, *196*, 29–42. [CrossRef]
35.  Otto, A.; Simoneit, B.R.T.; Rember, W.C. Conifer and Angiosperm Biomarkers in Clay Sediments and Fossil Plants from the Miocene Clarkia Formation, Idaho, USA. *Org. Geochem.* **2005**, *36*, 907–922. [CrossRef]
36.  Paul, S.; Sharma, J.; Singh, B.D.; Saraswati, P.K.; Dutta, S. Early Eocene Equatorial Vegetation and Depositional Environment: Biomarker and Palynological Evidences from a Lignite-Bearing Sequence of Cambay Basin, Western India. *Int. J. Coal Geol.* **2015**, *149*, 77–92. [CrossRef]
37.  van Aarssen, B.G.K.; Alexander, R.; Kagi, R.I. Higher Plant Biomarkers Reflect Palaeovegetation Changes during Jurassic Times. *Geochim. Cosmochim. Acta* **2000**, *64*, 1417–1424. [CrossRef]
38.  Ding, W.; Hou, D.; Gan, J.; Jiang, L.; Zhang, Z.; George, S.C. Sedimentary Geochemical Records of Late Miocene-Early Pliocene Palaeovegetation and Palaeoclimate Evolution in the Ying-Qiong Basin, South China Sea. *Mar. Geol.* **2022**, *445*, 106750. [CrossRef]
39.  Jiang, L.; George, S.C. Biomarker Signatures of Upper Cretaceous Latrobe Group Petroleum Source Rocks, Gippsland Basin, Australia: Distribution and Geological Significance of Aromatic Hydrocarbons. *Org. Geochem.* **2019**, *138*, 103905. [CrossRef]
40.  Samad, S.K.; Mishra, D.K.; Mathews, R.P.; Ghosh, S.; Mendhe, V.A.; Varma, A.K. Geochemical Attributes for Source Rock and Palaeoclimatic Reconstruction of the Auranga Basin, India. *J. Pet. Sci. Eng.* **2020**, *185*, 106665. [CrossRef]
41.  Cao, Z.; Liu, G.; Xiang, B.; Wang, P.; Niu, G.; Niu, Z.; Li, C.; Wang, C. Geochemical Characteristics of Crude Oil from a Tight Oil Reservoir in the Lucaogou Formation, Jimusar Sag, Junggar Basin. *AAPG Bull.* **2017**, *101*, 39–722. [CrossRef]
42.  Ding, X.; Gao, C.; Zha, M.; Chen, H.; Su, Y. Depositional Environment and Factors Controlling β-Carotane Accumulation: A Case Study from the Jimsar Sag, Junggar Basin, Northwestern China. *Palaeogeogr. Palaeoclimatol. Palaeoecol.* **2017**, *485*, 833–842. [CrossRef]
43.  Huang, W.-Y.; Meinschein, W.G. Sterols as Ecological Indicators. *Geochim. Cosmochim. Acta* **1979**, *43*, 739–745. [CrossRef]
44.  Volkman, J.K. Sterols and Other Triterpenoids: Source Specificity and Evolution of Biosynthetic Pathways. *Org. Geochem.* **2005**, *36*, 139–159. [CrossRef]
45.  Morford, J.L.; Emerson, S. The Geochemistry of Redox Sensitive Trace Metals in Sediments. *Geochim. Cosmochim. Acta* **1999**, *63*, 1735–1750. [CrossRef]
46.  Cao, J.; Wu, M.; Chen, Y.; Hu, K.; Bian, L.; Wang, L.; Zhang, Y. Trace and Rare Earth Element Geochemistry of Jurassic Mudstones in the Northern Qaidam Basin, Northwest China. *Geochemistry* **2012**, *72*, 245–2522. [CrossRef]
47.  Niu, Z.; Meng, W.; Wang, Y.; Wang, X.; Li, Z.; Wang, J.; Liu, H.; Wang, X. Characteristics of Trace Elements in Crude Oil in the East Section of the South Slope of Dongying Sag and Their Application in Crude Oil Classification. *J. Pet. Sci. Eng.* **2022**, *209*, 109833. [CrossRef]
48.  Shi, C.; Cao, J.; Luo, B.; Hu, W.; Tan, X.; Tian, X. Major Elements Trace Hydrocarbon Sources in Over-Mature Petroleum Systems: Insights from the Sinian Sichuan Basin, China. *Precambrian Res.* **2020**, *343*, 105726. [CrossRef]
49.  Wang, L.; Song, Z.; Yin, Q.; George, S.C. Paleosalinity Significance of Occurrence and Distribution of Methyltrimethyltridecyl Chromans in the Upper Cretaceous Nenjiang Formation, Songliao Basin, China. *Org. Geochem.* **2011**, *42*, 1411–1419. [CrossRef]
50.  Du, G.; Yang, Z.; Yin, H.; Wang, F.; Chen, Y.; Cui, Y. Developmental characteristics of organic matter and its enrichment model in shale reservoirs of Chang73 Member in Yanchang Formation of southeast Ordos Basin. *Pet. Geol. Recovery Effic.* **2022**, *29*, 1–11. (In Chinese with English Abstract)
51.  Chattopadhyay, A.; Dutta, S. Higher Plant Biomarker Signatures of Early Eocene Sediments of North Eastern India. *Mar. Pet. Geol.* **2014**, *57*, 51–67. [CrossRef]
52.  Jones, B.; Manning, D.A.C. Comparison of Geochemical Indices Used for the Interpretation of Palaeoredox Conditions in Ancient Mudstones. *Chem. Geol.* **1994**, *111*, 111–129. [CrossRef]

53. Wignall, P.B.; Twitchett, R.J. Oceanic Anoxia and the End Permian Mass Extinction. *Science* **1996**, *272*, 1155–1158. [CrossRef] [PubMed]

54. Awan, R.S.; Liu, C.; Gong, H.; Dun, C.; Tong, C.; Chamssidini, L.G. Paleo-Sedimentary Environment in Relation to Enrichment of Organic Matter of Early Cambrian Black Rocks of Niutitang Formation from Xiangxi Area China. *Mar. Pet. Geol.* **2020**, *112*, 104057. [CrossRef]

55. Fathy, D.; Wagreich, M.; Gier, S.; Mohamed, R.S.A.; Zaki, R.; El Nady, M.M. Maastrichtian Oil Shale Deposition on the Southern Tethys Margin, Egypt: Insights into Greenhouse Climate and Paleoceanography. *Palaeogeogr. Palaeoclimatol. Palaeoecol.* **2018**, *505*, 18–32. [CrossRef]

56. Hoş-Çebi, F. Organic Geochemical Characteristics and Paleoclimate Conditions of the Miocene Coals at the Çan-Durali (Çanakkale). *J. Afr. Earth Sci.* **2017**, *129*, 117–135. [CrossRef]